# Computational materials design for high-$T_c$ (Ga, Mn)As with Li codoping

L. Bergqvist[*]

*Department of Materials Science and Engineering, KTH Royal Institute of Technology, SE-100 44 Stockholm, Sweden*

K. Sato and H. Katayama-Yoshida

*Graduate School of Engineering Science, Osaka University, 1-3 Machikaneyama, Toyonaka, Osaka 560-8531, Japan*

P. H. Dederichs

*Peter Grünberg Institut, Forschungszentrum Jülich, DE-52425 Jülich, Germany*

(Received 11 October 2010; revised manuscript received 25 January 2011; published 7 April 2011)

Based on first-principles calculations and kinetic Monte Carlo simulations, we design a realistic and practical codoping technique for increasing the concentration of Mn atoms in GaAs and realizing high Curie temperatures in (Ga,Mn)As. We found that using codoping of Li interstitial atoms during the crystal growth has two great advantages. First, due to lower formation energy of Li interstitials compared to Mn interstitials, Li prevents formation of unwanted Mn interstitials. Second, Li interstitials can be removed by using post-growth annealing at low temperatures. This codoping method offers a general strategy to go far beyond the solubility limit and it should be applicable also to other diluted magnetic semiconductor systems.

DOI: 10.1103/PhysRevB.83.165201

PACS number(s): 75.50.Pp

## I. INTRODUCTION

Ferromagnetic dilute magnetic semiconductors such as $Ga_{1-x}Mn_xAs$ are hopeful materials for an all-semiconductor spintronics. However, the measured Curie temperature of 160 K in (Ga,Mn)As is much too low for realistic applications.[1,2] In these samples, Mn interstitials, which act as two-valent dopants and destroy the ferromagnetism, have been quantitatively removed by post-growth annealing of thin films.[1–4] While these samples have a nominal Mn concentration of about 7%, in samples with higher Mn concentrations, one would expect appreciably higher Curie temperatures $T_c$ since the Curie temperatures are for larger concentrations less affected by the percolation effect, which strongly reduces $T_c$ for dilute systems.[5–7] However, experiments with Mn concentrations of up to 20% show disappointingly low Curie temperatures,[8–13] indicating that there is a relatively large concentration of Mn interstitials that can not be removed by annealing. In this paper, we investigate by *ab initio* calculations the complex diffusion behavior of single Mn interstitials ($Mn_I$) in $Ga_{1-x}Mn_xAs$ samples with higher concentrations of substitutional Mn atoms ($Mn_S$). We find that, for higher Mn concentrations, an increasing number of $Mn_S$ dimers, trimers, and tetramers occur, which act as deeper traps for the $Mn_I$ interstitial, preventing the diffusion out of the sample and in this way strongly reducing the Curie temperature. As a way out, we recommend codoping during MBE growth with Li interstitials ($Li_I$). Similar to $Mn_I$, they strongly enhance the solubility of substitutional $Mn_S$ impurities and at the same time destroy the ferromagnetism. However, contrary to the $Mn_I$, they diffuse very fast[14] and are practically not trapped by $Mn_S$ clusters. Thus, they can be easily removed from relatively thick films by annealing and, in this way, should lead to ferromagnetic (Ga, Mn)As systems with higher $Mn_S$ concentrations and considerably higher Curie temperatures. A different, nevertheless somewhat similar, approach to high $T_c$ has been proposed by Mašek *et al.*[15]

After summarizing our calculation methods in Sec. II, we will discuss the effect of codoping in (Ga, Mn)As in Sec. III A by calculating the mixing energy. To discuss low-temperature annealing of codoped (Ga, Mn)As, first, energy landscapes and binding energies of $Li_I$ and $Mn_I$ with $Mn_S$ clusters are calculated in Sec. III B, then the diffusion length of interstitials in (Ga, Mn)As is estimated in Sec. III C. In Sec. IV, we summarize our computational design for high-$T_c$ (Ga, Mn)As.

## II. CALCULATION

The electronic structure calculations were performed using two different theoretical methods, the Korringa-Kohn-Rostoker (KKR) Green's function method and the projected augmented wave method (PAW). The diluted magnetic semiconductors (DMS) system is a disordered system. For example, in GaAs-based DMS, Ga atoms are randomly substituted by Mn impurities. In these calculations, this substitutional disorder is treated by using the coherent potential approximation (CPA). We use the KKR-CPA method employing the multipole-corrected atomic sphere approximation ($ASA + M$) (Ref. 16) with empty spheres included in the tetrahedral positions of the zinc-blende structure for a good space filling. Equal Wigner-Seitz radii were used for all spheres and the valence basis set consists of $spdf$ orbitals. For the valence orbitals, scalar relativistic corrections were taken into account, but spin-orbit effects were neglected. The core electrons were described by solving a fully relativistic Dirac equation. The local spin density approximation (LSDA) was employed for the exchange-correlation potential by using the parametrization of Perdew, Burke, and Ernzerhof (PBE).[17] In the KKR-CPA, the effective medium, which describes the configuration averaged disordered system, is calculated self-consistently within the single-site approximation. In this paper, the KKR-CPA method is conveniently used to calculate mixing energy of $Ga_{1-x}Mn_xAs$ and the effects of Li codoping on the mixing energy will be discussed in Sec. III A.

To discuss migration of the interstitial impurities, the energy landscape for diffusing interstitials should be calculated. In addition to the migration barrier, the diffusing interstitials should be trapped by the clusters formed by $Mn_S$ atoms. For calculating the energy landscape and the binding energies, we perform PAW calculations for supercells and use the "Vienna *ab initio* simulation package" (VASP).[18,19] For these calculations, the generalized gradient approximation (GGA) with PBE parametrization is used for the exchange-correlation potential.[17] Large supercells of either 128 or 250 atoms were employed. We performed test calculations with 432 atom supercells and confirmed that the results barely changed. $Mn_S$ atoms are distributed in the supercell by using special quasirandom structures proposed by Zunger *et al.*[20] An energy cutoff of 350 eV was chosen in all calculations. All atoms were allowed to relax until the atomic forces were smaller than 0.01 eV/Å. During atomic relaxations, a single $k$ point ($\Gamma$ point) was used, while the total energy in the final atomic configuration was calculated using a $2 \times 2 \times 2$ $k$-point grid and the tetrahedron method with Blöchl corrections. The energy landscape is calculated for a 128-atom supercell ($4 \times 4 \times 4$ conventional unit cell of the zinc-blende structure) by using the nudged elastic band (NEB) method.[21]

## III. DESIGN OF CODOPING METHOD FOR $Ga_{1-x}Mn_xAs$

### A. Mixing energy of $Mn_S$

As a starting point of our calculations, we discuss the formation energies of interstitial defects in GaAs and the binding energies of the considered complexes in (Ga,Mn)As. By using a 128-atom supercell, the formation energies of $Li_I$ and $Mn_I$ are caluated to be 1.0 and 3.3 eV, respectively. Thus, the formation energy of neutral interstitial $Li_I$ atoms in GaAs is considerably lower than the one for interstitial $Mn_I$ atoms. The equilibrium position of both interstitials is the tetrahedral position $T_{As}$ surrounded by four As atoms. When we introduce these interstitials into the dilute magnetic semiconductor $Ga_{1-x}Mn_xAs$, they act as single donors $Li_I^+$ in the case of Li interstitials or as double donors $Mn_I^{++}$ in the case of Mn interstitials, with the donor electrons filling up the hole states of the substitutional $Mn_S$ atoms, leading to a considerable gain of energy, but at the same time reducing the ferromagnetic exchange interaction.

To demonstrate this energy gain, we calculate within the coherent potential approximation (CPA) and by using the KKR-CPA method the mixing energy $E^{mix}(x)$ gained by mixing the system GaAs containing $y\%$ of interstitial defects $I_y$ on $T_{As}$ sites with the hypothetical 1-1 system of MnAs on zinc-blende lattice as a function of the $Mn_S$ concentration $x$. In the MBE crystal growth, the crystal structure of the epitaxial film is strongly affected by the structure of the substrate. In the (Ga, Mn)As case, its crystal structure is usually fixed to a zinc-blende structure. We are interested in high concentration doping in zinc-blende (Ga, Mn)As by preventing the phase decomposition. This is why we suppose the zinc-blende MnAs as a reference. $E^{mix}(x)$ is defined as

$$E^{mix}(x) = E[(Ga_{1-x}Mn_x)As - I_y]$$
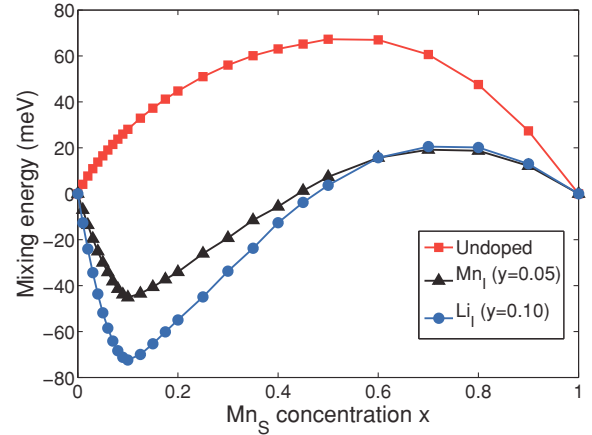$$- (1-x)E[GaAs - I_y] - xE[MnAs - I_y].$$



FIG. 1. (Color online) Mixing energies as a function of $Mn_S$ concentration $x$ for systems without and with interstitial atoms (Mn and Li, respectively).

Without interstitials, i.e., $y = 0$, the mixing energy $E^{mix}(x)$ is positive as shown in Fig. 1, indicating segregation behavior. This is in agreement with the fact that (Ga,Mn)As is always produced by nonequilibrium molecular beam epitaxy. However, for a finite concentration $y$ of interstitials, the mixing energy $E^{mix}(x)$ becomes negative as a function of the concentration $x$ of substitutional Mn impurities, meaning an increase of the Mn solubility. For given concentration $y$ of interstitials, the optimal gain in energy occurs for $x = y$ in the case of single-donor Li interstitials and $x = 2y$ for the double-donor Mn interstitials since, in this case, all hole states of the substitutional Mn impurities are filled by donor electrons. Thus, for a comparable effect of compensation, we have to compare, e.g., the curves for 5% Mn interstitials with 10% Li interstitials. Figure 1 shows that, in these cases, the largest reduction of the mixing energy occurs for 10% of $Mn_S$ impurities since, in this case, all Mn hole states are filled and no additional energy can be gained. From experiment, it is well known that, at a sufficient concentration of $Mn_S$ impurities, interstitial $Mn_I$ impurities are formed spontaneously, which is in agreement with the above results.[1] However, Fig. 1 also shows that Li interstitials lead to a larger energy gain. Thus, in codoping experiments, Li interstitials should suppress the formation of Mn interstitials. Moreover, as we will show below, they can be more easily removed from the sample by annealing.

### B. Energy landscape of diffusing $Li_I$ and $Mn_I$

We will now discuss the annealing behavior and the related diffusion process of the interstitial atoms. In Fig. 2, migration barriers are calculated for $Li_I$ and $Mn_I$. The migration path $T_{As} \rightarrow T_{Ga} \rightarrow T_{As}$ has a double bump structure with a maximum at the hexagonal positions and a metastable minimum at the intermediate $T_{Ga}$ position as in Ref. 23. We find that, for the fully ionized $Mn_I^{++}$ interstitial, we find a migration barrier of about 0.7 eV, which is in good agreement with experiments[1,22] and previous calculations,[1,23] more or less independent of the approximation used (LDA, GGA, or GGA + U). For the $Li^+$ ion, the same behavior is found, however, with a smaller barrier of about 0.5 eV.
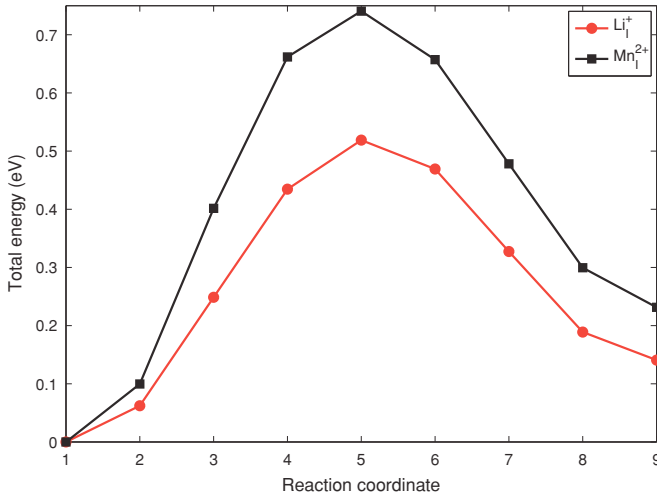
FIG. 2. (Color online) Energy landscape from nudged elastic band (NEB) calculations for a diffusing $Li_I^+$ (red filled circle) and $Mn_I^{2+}$ (black filled squares) in GaAs along two tetrahedral interstitial sites $T_{As}$ (reaction coordinate 1) and $T_{Ga}$ (reaction coordinate 9), which are surrounded by four Ga and four As atoms, respectively, via a hexagonal interstitial site (reaction coordinate 5).

For the annealing process, the trapping behavior of the "free" interstitial ion at substitutional $Mn_S$ impurities and $Mn_S$ clusters is most important, since basically the trapping and detrapping energies at these $Mn_S$ impurities and $Mn_S$ clusters determine the diffusion behavior. Even for a random distribution of $Mn_S$ impurities, such clusters occur for any finite concentration $x$. The probability that, in such a sea of randomly distributed $Mn_S$ impurities, the interstitial at a position $T_{Ga}$ is trapped by $n$ neighboring $Mn_S$ atoms on Ga sites, i.e., by a single $Mn_S$ atom for $n = 1$, by a nearest-neighbor dimer ($n = 2$), a triangular trimer ($n = 3$), or a compact tetrahedral tetramer ($n = 4$), can be easily calculated and is given by $P_n(x) = \binom{4}{n} x^n (1 - x)^{4-n}$.

Thus, for a $Mn_S$ concentration of 5% ($x = 0.05$), an interstitial can perform about four free jumps ($P_0 = 0.81$) before it is trapped at a single $Mn_S$ interstitial ($P_1 = 0.18$), and only about every 70th step it meets a $Mn_S$ dimer ($P_2 = 0.014$) and a trimer only after about 2000 steps ($P_3 = 0.0005$). On the other hand, for 20% $Mn_S$, the situation is completely different: after about two to three diffusion steps, the interstitial is trapped at a single $Mn_S$ ($P_1 = 0.41$), about every 7th step at a dimer ($P_2 = 0.15$) and every 40th step at a $Mn_S$ trimer ($P_3 = 0.026$). Thus, the higher order complexes and the binding energies at these complexes play an increasingly larger role for increasing concentrations and have to be calculated.

Figures 3(a) and 3(c) show the energy landscape for a diffusing $Li_I^+$ interstitial [Fig. 3(a)] and $Mn_I^{++}$ interstitial [Fig. 3(c)] close to a single $Mn_S$ impurity using a 128-atom supercell. Both the GGA as well as the GGA + U method (using $U = 4$ eV and $J = 0.8$ eV for the Mn $d$ states) give practically the same results and we show only the GGA + U result in the figure. The coordinates of $Mn_S$ and the interstitial impurities used for the NEB calculations are tabulated in Table I and visualized in Fig. 4. The energetically lowest configuration is either the nearest-neighbor $T_{Ga}$ interstitial position or a close $T_{As}$ position [Nos. 5 and 9 in Figs. 3(a)
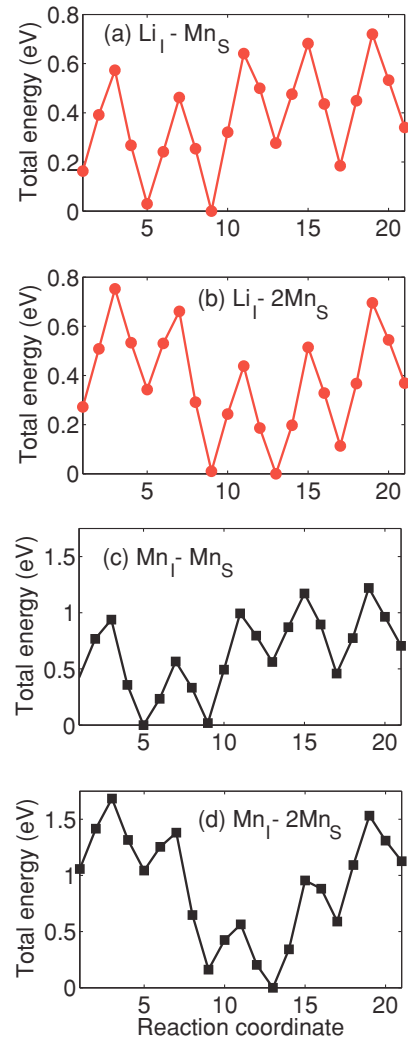


FIG. 3. (Color online) Energy landscape from nudged elastic band (NEB) calculations for a diffusing interstitial atom in proximity to $Mn_S$ atoms. In (a) and (b), a $Li_I$ is diffusing in proximity of 1 and 2 $Mn_S$, respectively. In (c) and (d), a $Mn_I$ is diffusing in proximity of 1 and 2 $Mn_S$, respectively. The coordinates on the horizontal axis are listed in Table I.

TABLE I. The Mn coordinates (direct coordinates) in the 128-atom supercell ($4 \times 4 \times 4$ zinc-blende structure) used in the NEB calculations. $S$ denotes the substitutional position and positions 1–21 are the different interstitial positions used in the calculation of the energy landscapes for the diffusion paths of Figs. 3(a)–3(d).

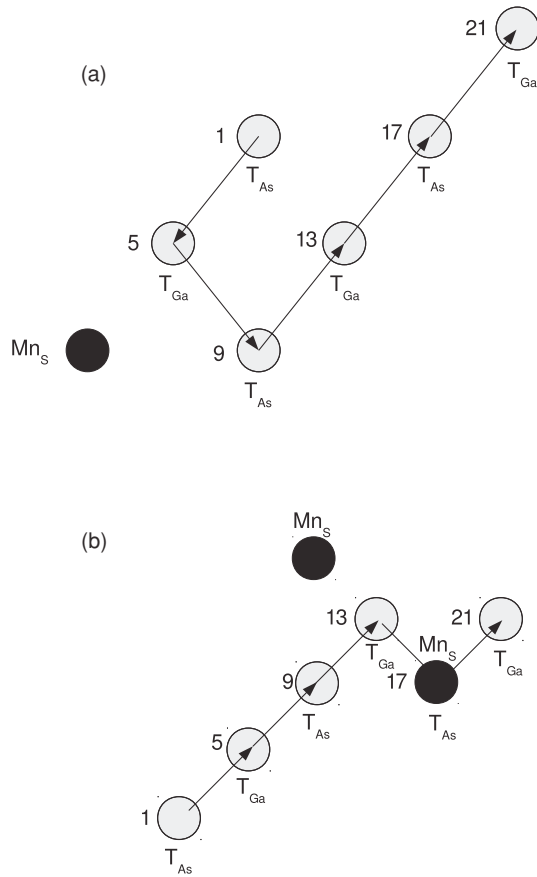| Mn positions | Coordinates | | | Coordinates | | |
|---|---|---|---|---|---|---|
| $S1$ | 0.7500 | 0.2500 | 0.5000 | 0.7500 | 0.2500 | 0.7500 |
| $S2$ | | | | 0.5000 | 0.5000 | 0.7500 |
| 1 | 0.6250 | 0.1250 | 0.8750 | 0.6250 | 0.3750 | 0.3750 |
| 5 | 0.6875 | 0.1875 | 0.6875 | 0.6875 | 0.4375 | 0.4375 |
| 9 | 0.6250 | 0.3750 | 0.6250 | 0.6250 | 0.3750 | 0.6250 |
| 13 | 0.6875 | 0.4375 | 0.6875 | 0.6875 | 0.4375 | 0.6875 |
| 17 | 0.6250 | 0.3750 | 0.8750 | 0.6250 | 0.6250 | 0.6250 |
| 21 | 0.6875 | 0.4375 | 0.9375 | 0.6875 | 0.6875 | 0.6875 |

FIG. 4. (Color online) Graphical illustration of the pathway of the interstitial atom (gray) used for NEB calculations visualized on a two-dimensional plane. The $Mn_S$ atoms are displayed in black and are fixed in the calculation. Part (a) shows the path with 1 $Mn_S$ and (b) shows the case of 2 $Mn_S$. The corresponding energy landscape is shown in Figs. 3(a)–3(d).

and 3(c)]; both are more or less degenerate. The $T_{Ga}$ position No. 21 is farthest away from the trapping $Mn_S$ impurity and determines the binding energy, which is about 0.6 eV for $Mn_I$, but only 0.3 eV for $Li_I$. [If the $Mn_S$ impurity is located at (0.750, 0.250, 0.500), the coordinates of the interstitial position 21 are (0.688, 0.438, 0.938)]. In Figs. 3(b) and 3(d), we present the corresponding energy landscapes for the trapping at the $(Mn_S)_2$ dimer. The coordinates of the second $Mn_S$ dimer atom are (0.500, 0.500, 0.750). The coordinates of the positions along the diffusion energies for the $Mn_I$ interstitials are increased to more than 1 eV, while the binding of $Li_I$ of about 0.4 eV is still rather small. Figure 5 summarizes the results for the binding energies of $Mn_I^{++}$ and $Li_I^+$ interstitials at single $Mn_S$ impurities, and at impurities dimers, trimers, and tetramers. All calculations were performed for the substitutional cluster and the interstitial atom was placed in the most stable configuration and at maximum separation within a 250-atom supercell. One trend is very obvious: The binding energies of the Li interstitials increase only rather moderately with cluster size. Taking this together with the low diffusion energy, the Li interstitial should have no problem diffusing through the sample, even for high concentrations of $Mn_S$. We demonstrate this in diffusion simulations below. The reason

for the low binding is basically the pronounced electrostatic nature of the interaction. In a rough approximation, the binding energy arises from the electrostatic attraction of the $Li^+$ ion with the negative screening charges in the hole state of neighboring $Mn_S$ impurities. In the electrostatic picture, the binding is the same if the screening charge is distributed on one or more $Mn_S$ impurities, as long as the distances to the $Li^+$ ion are the same.

In contrast to this behavior, the interaction of the $Mn^{++}$ interstitial strongly increases with cluster size. Here the interaction is dominated by the covalent hybridization of the Mn $d$ states, which leads to a strong increase with cluster size. In the GGA $+ U$ approach, the majority of $d$ states of Mn are shifted to lower energies, i.e., to a region of about $-4$ eV below $E_F$,[7,24] in agreement with photoemission measurements giving a peak at $-4.2$ eV. Therefore, the GGA $+ U$ results, giving considerably lower binding energies and exchange interactions being dominated by $p$-$d$ exchange,[7,24] should be more realistic. Thus, this decrease of the binding is a consequence of the more localized behavior of the Mn $d$ states, which partly suppresses the covalent binding. However, compared to the case of $Li^+$ interstitials, the binding energies are still very high. As we will demonstrate in the following, these binding energies prevent the out diffusion of Mn interstitials for higher concentrations of $Mn_S$, thus representing a serious obstacle for higher $T_c$ values at larger concentrations. On the other hand, our calculations indicate that this problem does not occur for Li dopants, so that it should be possible to achieve Curie temperatures for (Ga, Mn)As systems with high concentrations of Mn.

One might worry about whether some secondary phases would be formed due to the intense doping of Li in addition to Mn. Fortunately, there exists the ternary compound LiMnAs, which is antiferromagnetic. LiMnAs shows a filled zinc-blende structure, namely, MnAs forms a zinc-blende lattice and all of its $T_{As}$ interstitial sites are occupied by Li.[15] The existence of this compound partially guarantees the reality of our design of Li codoping.
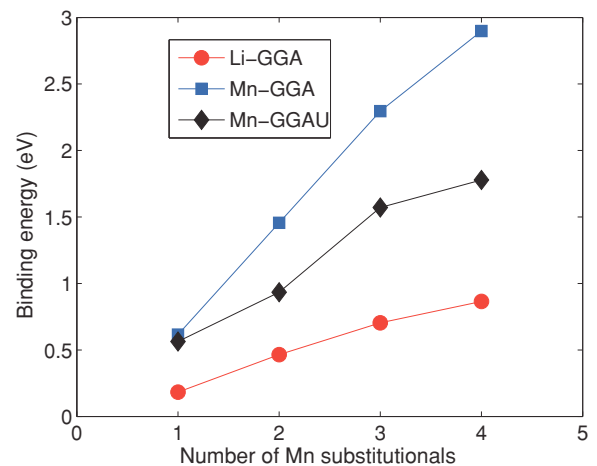


FIG. 5. (Color online) Binding energies of Li and Mn interstitials in presence to 1–4 $Mn_S$ impurities. In the case of $Mn_I$ interstitials, both the GGA and GGA $+ U$ results are shown.

### C. Post-growth annealing of (Ga, Mn)As

For designing post-growth annealing of codoped (Ga, Mn)As, we have to discuss the trap-limited diffusion of $Mn_I$ and $Li_I$ in (Ga,Mn)As quantitatively, namely, we calculate effective diffusion constants of the interstitial impurities under the existence of $Mn_S$ clusters as trapping sites. As a straightforward approach, we perform random walk simulations by using the Monte Carlo technique in this paper. The interstitial impurities diffuse in the crystal by climbing up the migration barrier. When the interstitial impurity comes to the nearest-neighbor $Mn_S$ sites, it has to overcome the binding energy in addition to the migration barrier to escape from the trapping site.

For the migration barrier, we use experimental values, which are 0.7 eV for $Mn_I$ and 0.67 eV for $Li_I$. For realistic distribution of trapping sites, we prepare a $10 \times 10 \times 10$ supercell of conventional cubic unit cells of GaAs (zinc-blende structure) and distribute Mn impurities on Ga sublattices. The interstitial impurities hop alternatively on $T_{As}$ and $T_{Ga}$ sites. At $T_{Ga}$ sites, depending on the number of nearest-neighbor $Mn_S$, we consider the calculated binding energies shown in Fig. 5. The random walk simulations are repeated $10^4$ times for one supercell with the periodic boundary condition, and we consider 50 different supercells for configuration averaging. In order to accelerate the simulation, we utilize the variable time technique.[25] The estimated effective diffusion constant $D_{eff}$ corresponds well to the phenomenological estimation.[26]

To estimate annealing depth of interstitial impurities in (Ga,Mn)As, we assume an infinite drain for interstitials at the surface of (Ga,Mn)As. This is actually the case for $Mn_I$,[1] and, for $Li_I$, this assumption is reasonable due to the reactive nature of the Li atom. Under this assumption, the annealing depth $d$ after time $t$ is calculated as $d = \sqrt{D_{eff} t}$. $d$ is measured from the sample surface and defined as the depth at which the concentration of the diffusing impurity becomes half of the initial concentration.

Assuming an annealing time of 24 hours, we give some numbers for the estimated annealing depths in Table II. Due to the large binding energies, out diffusion of $Mn_I$ is already difficult for low concentrations. Considering the typical film thickness of 10–100 nm, the annealing temperature should be higher than 500 K to realize reasonable annealing depths of $Mn_I$. At these temperatures, the annealing depths of $Li_I$ are about three orders of magnitude larger and the advantage of $Li_I$ is apparent. Even for 30% of $Mn_S$ at 444 K, the

annealing depth of $Li_I$ reaches 120 nm, which is enough for diffusing out from the (Ga,Mn)As. The complete out diffusion of $Li_I$ would lead to a dramatic increase of $T_c$ for higher concentrations of $Mn_S$. Monte Carlo simulations of $T_c$ based on LDA $+ U$ calculations give for 8% Mn a Curie temperature of 114 K, in good agreement with experiment, but predict for 20% or 30% Mn Curie temperatures of 314 or 468 K. We have also calculated the potential energy profile of Mn from the Ga substitutional site to the nearest tetrahedral interstitial site. The calculated energy barrier is higher than 2 eV, and this process (diffusion of Mn from substitutional to interstitial site) is not likely to occur at the present annealing temperatures.

It was already demonstrated that the low-temperature post annealing was effective to increase Curie temperature, in particular, in Ref. 13 entire removal of Mn interstitials from (Ga, Mn)As was claimed. However, in these experiments, Mn concentration is still low ($\sim$9%). Therefore, at very high concentrations, which is required for high $T_c$, the removal of $Mn_I$ is not probable and it is particularly advantageous to use $Li_I$ as codopants. Moreover, as shown in Fig. 1, $Li_I$ interstitials lower the mixing energy of $Mn_S$ much more than the $Mn_I$. This means that $Li_I$ reduces the concentration of $Mn_I$, resulting in higher $Mn_S$ concentration.

$Li_I$ can diffuse to the surface during the epitaxial growth; however, the epitaxial technique is a highly nonequilibrium one and Li vapor is continuously supplied from the source. This causes the increase of chemical potential of Li outside the sample, and we can expect Li inclusion into the sample up to the required concentration for the effectiveness of codoping. On the other hand, during a post-growth annealing, the Li flux is switched off and we can not expect a supply of Li from outside. Since Li is highly reactive and oxidized at the surface, it is safely supposed that the surface works as a drain of Li. The effect of the surface has been discussed in Ref. 1. This is why the Li codoping works during the epitaxial growth and the post-growth annealing is effective to remove Li impurities.

## IV. SUMMARY

We have performed first-principles calculations of the formation energy of $Mn_I$ and $Li_I$ interstitials, their energy landscapes in concentrated (Ga,Mn)As, and Monte Carlo simulations of the interstitial diffusion. It is found that the codoping of $Li_I$ during the crystal growth of (Ga,Mn)As has two advantages. Due to the lower formation energy of $Mn_S$-$Li_I$ complexes compared to $Mn_S$-$Mn_I$, we can dope $Mn_S$ up to high concentrations by avoiding $Mn_I$ formation. $Li_I$ can be removed by using post-growth annealing at low temperature owing to the small binding energies between $Li_I$ and $Mn_S$ clusters. On the basis of these results, we design a realistic and practical codoping technique for increasing concentration of $Mn_S$ and realizing high Curie temperature in (Ga,Mn)As. Since the ferromagnetism in dilute magnetic semiconductor systems is carrier mediated, every DMS system should show saturation of $T_c$ for high concentrations due to the self-compensation. The present codoping method offers a general strategy to go far beyond the solubility limit by avoiding the compensation so that this method should be applicable also to systems other than (Ga,Mn)As.

TABLE II. Calculated annealing depth of $Li_I$ and $Mn_I$ in (Ga, Mn)As. 24 hours annealing is assumed.

| | Annealing depth $= \sqrt{D_{eff} t}$ ($\mu$m) | | | | | |
|---|---|---|---|---|---|---|
| | Interstitial Li | | | Interstitial Mn | | |
| $Mn_S$ | 444 (K) | 500 (K) | 571 (K) | 444 (K) | 500 (K) | 571 (K) |
| 1% | 8.53 | 41.36 | 174.17 | 0.00 | 0.03 | 0.39 |
| 2% | 3.90 | 20.63 | 99.66 | 0.00 | 0.02 | 0.19 |
| 5% | 1.24 | 7.09 | 37.99 | 0.00 | 0.01 | 0.07 |
| 7% | 0.80 | 4.65 | 25.60 | 0.00 | 0.00 | 0.05 |
| 15% | 0.28 | 1.73 | 9.99 | 0.00 | 0.00 | 0.02 |
| 30% | 0.12 | 0.71 | 4.21 | 0.00 | 0.00 | 0.01 |

*lbergqv@kth.se

[1] K. W. Edmonds, P. Boguslawski, K. Y. Wang, R. P. Campion, S. N. Novikov, N. R. S. Farley, B. L. Gallagher, C. T. Foxon, M. Sawicki, T. Dietl, M. Buongiorno Nardelli, and J. Bernholc, Phys. Rev. Lett. **92**, 037201 (2004).

[2] D. Chiba, K. Takamura, F. Matsukura, and H. Ohno, Appl. Phys. Lett. **82**, 3020 (2003).

[3] T. Hayashi, Y. Hashimoto, S. Katsumoto, and Y. Iye, Appl. Phys. Lett. **78**, 1691 (2001).

[4] S. J. Potashnik, K. C. Ku, S. H. Chun, J. J. Berry, N. Samarth, and P. Schiffer, Appl. Phys. Lett. **79**, 1495 (2001).

[5] L. Bergqvist, O. Eriksson, J. Kudrnovský, V. Drchal, P. Korzhavyi, and I. Turek, Phys. Rev. Lett. **93**, 137202 (2004).

[6] K. Sato, W. Schweika, P. H. Dederichs, and H. Katayama-Yoshida, Phys. Rev. B **70**, 201202(R) (2004).

[7] K. Sato, L. Bergqvist, J. Kudrnovský, P. H. Dederichs, O. Eriksson, I. Turek, B. Sanyal, G. Bouzerar, H. Katayama-Yoshida, V. A. Dinh, T. Fukushima, H. Kizaki, and R. Zeller, Rev. Mod. Phys. **82**, 1633 (2010).

[8] D. Chiba, Y. Nishitani, F. Matsukura, and H. Ohno, Appl. Phys. Lett. **90**, 122503 (2007).

[9] S. Ohya, K. Ohno, and M. Tanaka, Appl. Phys. Lett. **90**, 112503 (2007).

[10] M. Wang, R. P. Campion, A. W. Rushforth, K. W. Edmonds, C. T. Foxon, and B. L. Gallagher, Appl. Phys. Lett. **93**, 132103 (2008).

[11] S. Mack, R. C. Myers, J. T. Heron, A. C. Gossard, and D. D. Awschalom, Appl. Phys. Lett. **92**, 192502 (2008).

[12] L. Chen, S. Yan, P. F. Xu, J. Lu, W. Z. Wang, J. J. Deng, X. Qian, Y. Ji, and J. H. Zhao, Appl. Phys. Lett. **95**, 182505 (2009).

[13] D. Chiba, K. M. Yu, W. Walukiewica, Y. Nishitani, F. Matsukura, and H. Ohno, J. Appl. Phys. **103**, 07D136 (2008).

[14] K. Leosson and H. P. Gislason, Phys. Rev. B **56**, 9506 (1997).

[15] J. Mašek, J. Kudrnovský, F. Máca, B. L. Gallagher, R. P. Campion, D. H. Gregory, and T. Jungwirth, Phys. Rev. Lett. **98**, 067202 (2007).

[16] A. V. Ruban, S. I. Simak, P. A. Korzhavyi, and H. L. Skriver, Phys. Rev. B **66**, 024202 (2002).

[17] J. P. Perdew, K. Burke, and M. Ernzerhof, Phys. Rev. Lett. **77**, 3865 (1996).

[18] G. Kresse and J. Furthmüller, Phys. Rev. B **54**, 11169 (1996).

[19] G. Kresse and D. Joubert, Phys. Rev. B **59**, 1758 (1999).

[20] A. Zunger, S.-H. Wei, L. G. Ferreira, and J. E. Bernard, Phys. Rev. Lett. **65**, 353 (1990).

[21] D. Sheppard, R. Terrel, and G. Henkelman, J. Chem. Phys. **128**, 134106 (2008).

[22] R. E. Goacher, S. Hegde, H. Luo, and J. A. Gardella Jr., J. Appl. Phys. **106**, 044302 (2009).

[23] V. I. Baykov, P. A. Korzhavyi, and B. Johansson, Phys. Rev. Lett. **101**, 177204 (2008).

[24] K. Sato, P. H. Dederichs, H. Katayama-Yoshida, and J. Kudrnovsky, J. Phys. Condens. Matter **16**, S5491 (2004).

[25] M. E. J. Newman and G. T. Barkema, *Monte Carlo Methods in Statistical Physics* (Oxford University, New York, 1999).

[26] P. A. Fedders, Phys. Rev. B **16**, 4769 (1977).